The RING-Type E3 Ligase XBAT35.2 Is Involved in Cell Death Induction and Pathogen Response[1][OPEN]

Hongxia Liu,[a] Sridhar Ravichandran,[b,2] Ooi-kock Teh,[c,3] Sarah McVey,[a] Carly Lilley,[a] Howard J. Teresinski,[d,4] Carmen Gonzalez-Ferrer,[a] Robert T. Mullen,[d] Daniel Hofius,[c] Balakrishnan Prithiviraj,[b] and Sophia L. Stone[a,5]

[a]Biology Department, Dalhousie University, Halifax, Nova Scotia, Canada B3H 4R4
[b]Department of Plant, Food, and Environmental Sciences, Agricultural Campus, Dalhousie University, Truro, Nova Scotia, Canada B2N 5E3
[c]Department of Plant Biology, Uppsala BioCenter, Swedish University of Agricultural Sciences (SLU) and Linnean Center for Plant Biology, SE-75007 Uppsala, Sweden
[d]Department of Molecular and Cellular Biology, Summerlee Science Complex, University of Guelph, Guelph, Ontario, Canada N1G 2W1

ORCID IDs: 0000-0001-6800-2748 (O.-k.T.); 0000-0002-6915-7407 (R.T.M.); 0000-0002-4854-9946 (D.H.); 0000-0003-2140-6037 (S.L.S.).

XBAT35 belongs to a subfamily of Arabidopsis (*Arabidopsis thaliana*) RING-type E3s that are similar in domain architecture to the rice (*Oryza sativa*) XA21 Binding Protein3, a defense protein. The *XBAT35* transcript undergoes alternative splicing to produce two protein isoforms, XBAT35.1 and XBAT35.2. Here, we demonstrate that XBAT35.2 localizes predominantly to the Golgi and is involved in cell death induction and pathogen response. XBAT35.2, but not XBAT35.1, was found to trigger cell death when overexpressed in tobacco (*Nicotiana benthamiana*) leaves and does so in a manner that requires its RING domain. Loss of *XBAT35* gene function disrupts the plant's ability to defend against pathogen attack, whereas overexpression of *XBAT35.2* enhances resistance to pathogens. XBAT35.2 was found to be unstable and promotes its own degradation, suggesting self-regulation. Inoculation with virulent and avirulent strains of the bacterial pathogen *Pseudomonas syringae* pv *tomato* DC3000 results in a drastic reduction in the levels of ubiquitinated XBAT35.2 and an increase in the abundance of the E3. This implies that pathogen infection prohibits XBAT35.2 self-regulation and stabilizes the E3. In agreement with a role in defending against pathogens, XBAT35.2 interacts with defense-related Accelerated Cell Death11 (ACD11) in planta and promotes the proteasome-dependent turnover of ACD11 in cell-free degradation assays. In accordance with regulation by a stabilized XBAT35.2, the levels of ubiquitinated ACD11 increased considerably, and the abundance of ACD11 was reduced following pathogen infection. In addition, treatment of transgenic seedlings with a proteasome inhibitor results in the accumulation of ACD11, confirming proteasome-dependent degradation. Collectively, these results highlight a novel role for XBAT35.2 in cell death induction and defense against pathogens.

[1] This research was supported by grants from the Natural Science and Engineering Research Council of Canada (NSERC) to S.L.S., R.T.M., and B.P. H.J.T. was supported by an Ontario Graduate Scholarship, and S.M. was supported by a NSERC Canada Graduate Scholarships-Master's (CGS M) scholarship.

[2] Current address: Agriculture and Agri-Food Canada, Ottawa, Ontario, Canada K1A 0C6.
[3] Current address: Institute for International Collaboration, Hokkaido University, Sapporo 060-0815, Japan, and Department of Biological Science, School of Science, Hokkaido University, Sapporo 060-0810, Japan.
[4] Current address: Department of Biology, Queen's University, Kingston, Ontario, Canada K7L 3N6.
[5] Address correspondence to sophia.stone@dal.ca.
The author responsible for distribution of materials integral to the findings presented in this article in accordance with the policy described in the Instructions for Authors (www.plantphysiol.org) is: Sophia L. Stone (sophia.stone@dal.ca).

S.L.S., R.T.M., D.H., and B.P. designed the research; H.L., S.M., O.-k.T., S.R., C.L., C.G.-F., and H.J.T. performed experiments; all authors analyzed data; H.L. and S.L.S. wrote the article; S.L.S., R.T.M., D.H., and B.P. edited the article.

[OPEN] Articles can be viewed without a subscription.
www.plantphysiol.org/cgi/doi/10.1104/pp.17.01071

Posttranslational modification (PTM) via ubiquitination plays essential regulatory roles in all eukaryotic cells. The selective attachment of ubiquitin serves as a versatile modification that regulates protein activity, abundance, sorting, and localization (Deshaies and Joazeiro, 2009; Komander and Rape, 2012). This versatility places ubiquitination at the center of numerous cellular processes and allows for the regulation of growth, development, and responses to various environmental stimuli. Ubiquitination is accomplished through the sequential action of three enzymes: E1 (ubiquitin-activating enzyme), E2 (ubiquitin-conjugating enzyme), and E3 (ubiquitin ligase). Ubiquitin conjugation begins with the activation of ubiquitin molecules by E1, which is then transferred to E2, forming a thioester-linked E2-ubiquitin intermediate. Finally, E3 mediates the transfer of ubiquitin from the E2-ubiquitin intermediate to the substrate. The covalent attachment of ubiquitin to the substrate is usually accomplished via the formation of an isopeptide bond between the C-terminal Gly of ubiquitin and an internal lysine (Lys) of the substrate. Substrate modifications include the

attachment of a single ubiquitin (monoubiquitination), multiple ubiquitin molecules (multimonoubiquitination), or a polyubiquitin chain (polyubiquitination). Ubiquitin contains seven internal Lys residues, all of which can be used to assemble structurally diverse polyubiquitin chains (Peng et al., 2003; Xu et al., 2009). Each type of modification facilitates a different outcome; for example, a monoubiquitinated substrate may be shuttled from the nucleus to the cytoplasm, the attachment of a Lys-63-linked polyubiquitin chain has been linked to protein activation, and the assembly of a Lys-48-linked chain targets the substrate for degradation by the 26S proteasome, a multiproteolytic complex (Chau et al., 1989; Deng et al., 2000; Thrower et al., 2000; Carter et al., 2007).

The hierarchical nature of the ubiquitination pathway is reflected in the number of each ubiquitin enzyme. Eukaryotic genomes usually contain one or two E1s, tens of E2s, and hundreds of E3s. The Arabidopsis (*Arabidopsis thaliana*) genome, for example, contains two E1 isoforms, 47 E2s, and over 1,400 E3s (Smalle and Vierstra, 2004; Kraft et al., 2005), the large number of the latter reflecting their role as the determinants of substrate specificity within the ubiquitination pathway. Biochemical and transgenic studies have allowed for the assignment of biological functions to a growing number of E3 ligases (Vierstra, 2009; Sadanandom et al., 2012; Stone, 2014). However, knowledge of the proteins targeted by E3 ligases is largely lacking. The identification of these interacting proteins is important, since they may serve as targets for ubiquitination and, thus, are required to fully understand the biological functions of the E3 ligases. Also, interacting proteins may function as regulators that modulate E3 ligase activity. Here, we report on our results obtained using various approaches to identify a substrate protein for XBAT35 (XB3 ortholog5 in Arabidopsis), a member of the ankyrin repeat-containing subfamily of Really Interesting New Gene (RING)-type E3 ligases (RING-ankyrin).

The six members of the Arabidopsis RING-ankyrin E3 ligase subfamily, XBAT31 to XBAT36, were identified based on similarity in amino acid sequence and domain organization to rice (*Oryza sativa*) XB3 (XA21 Binding Protein3), an E3 ligase that promotes defense against pathogen attack (Nodzon et al., 2004; Wang et al., 2006). The RING-ankyrin proteins from Arabidopsis and other plant species all contain a series of N-terminal ankyrin repeats that facilitate protein-protein interactions followed by a RING-HCa E3 ligase domain (Nodzon et al., 2004; Stone et al., 2006; Huang et al., 2013; Yuan et al., 2013). Ubiquitin ligase activity and function have been demonstrated for two members, XBAT32 and XBAT35, the former being involved in regulating ethylene biosynthesis and lateral root development, while the latter is thought to maintain apical hook curvature (Nodzon et al., 2004; Stone et al., 2006; Prasad et al., 2010; Prasad and Stone, 2010; Carvalho et al., 2012). Biologically relevant substrate proteins have been identified also for XBAT32, which attaches ubiquitin to the ethylene biosynthesis enzymes 1-Aminocyclopropane-1-Carboxylic Acid Synthase7 (ACS7) and ACS4 (Lyzenga et al., 2012). The *XBAT35* gene is known to be alternatively spliced, yielding two protein isoforms, a larger, nucleus-localized XBAT35.1 and a smaller, cytoplasm-localized XBAT35.2 (Carvalho et al., 2012). However, substrate proteins have not been identified for either XBAT35 isoform. A high-throughput yeast two-hybrid (Y2H) screen placed XBAT35 within a protein-protein interaction network that included Accelerated Cell Death11 (ACD11). Loss of *ACD11* function leads to constitutive activation of programmed cell death and defense response pathways in the absence of pathogen attack (Brodersen et al., 2002; Petersen et al., 2009; Braun et al., 2011).

Here, we demonstrate that XBAT35.2 induces cell death when expressed transiently in tobacco (*Nicotiana benthamiana*) leaf, suggesting a functional link between this isoform and ACD11. In addition, loss of *XBAT35* function impaired the plant's ability to properly defend against pathogens, while overexpression of *XBAT35.2* enhanced resistance. Our results confirm the in planta interaction between the Golgi-localized XBAT35.2 and ACD11 and also provide evidence that XBAT35.2 mediates the proteasome-dependent degradation of ACD11. Pathogen infection stabilizes autoubiquitinating XBAT35.2 and promotes the ubiquitination and subsequent degradation of ACD11. These results suggest a model where, in the absence of pathogen, XBAT35.2 levels are kept low via self-regulation and ACD11 is able to accumulate and inhibit cell death. In the presence of pathogen, XBAT35.2 accumulation would promote ACD11 degradation, allowing for cell death to occur as part of the defense response to pathogen infection. Overall, the assessment of interacting proteins has allowed us to further characterize XBAT35.2 by identifying a novel role for the E3 ligase in plant defense against pathogen attack.

RESULTS

XBAT35.2 Interacts with ACD11 in Planta

Arabidopsis protein-protein interactomes generated using Y2H screens have placed the RING-type E3 XBAT35 within an interaction network that includes Prenylated RAB Acceptor1.F proteins (PRA1.F2–PRA1.F4), which interact with ACD11 and Binding Partner of ACD11, and COP9 signalosome complex subunit 5a (Petersen et al., 2009; Braun et al., 2011). To determine if PRA1.F2 to PRA1.F4, ACD11, or other proteins within the network may serve as potential substrates for XBAT35, we utilized various assays to confirm interaction with the ubiquitin ligase. Here, we report on our analysis of the interaction between E3 and ACD11. *XBAT35* is expressed as two isoforms, XBAT35.1 and XBAT35.2 (Carvalho et al., 2012); however, the identity of the isoform(s) used in the high-throughput interaction screens was not reported (Braun et al., 2011). As shown in Supplemental Figure S1A, confocal microscopy analysis of *Agrobacterium tumefaciens*-mediated, transiently transformed tobacco

leaf epidermal cells revealed that yellow fluorescent protein (YFP)- and hemagglutinin (HA) epitope-tagged XBAT35.1 (XBAT35.1-YFP-HA) resided exclusively in the nucleus, confirming previous reports on its intracellular localization (Carvalho et al., 2012). On the other hand, XBAT35.2-YFP-HA and a modified version of the protein, namely XBAT35.2^{AA}-YFP-HA, which lacks E3 ligase activity due to two amino acid point mutations (i.e. substitutions with Ala) in the RING domain (Kraft et al., 2005; Stone et al., 2005; Carvalho et al., 2012), as well as ACD11-YFP-HA, were observed throughout the cytoplasm and in discrete punctate structures in tobacco leaf cells (Supplemental Fig. S1, B–D). These similarities in the localization patterns of XBAT35.2 (and XBAT35.2^{AA}) and ACD11 suggest that the two proteins are at least proximal to one another in plants and, therefore, could interact. To assess the in planta interaction between XBAT35.2 and ACD11, intracellular colocalization, bimolecular fluorescence complementation (BiFC), and immunoprecipitation (IP) assays were employed. XBAT35.2^{AA} was used in in vivo assays to ensure that any potential interacting proteins are not modified and degraded by the proteasome. As shown in Figure 1A, cyan fluorescent protein (CFP)- and HA-tagged XBAT35.2^{AA} (XBAT35.2^{AA}-CFP-HA) and ACD11-YFP-HA fusion proteins colocalized primarily at punctate structures in transiently cotransformed tobacco leaf cells. As a control, tobacco epidermal cells expressing XBAT35.2^{AA}-CFP-HA or ACD11-YFP-HA alone were assessed to ensure that no fluorescence signal overlap occurred between the YFP and CFP channels (Fig. 1, B and C).

For BiFC assays, both candidate proteins were coexpressed (via *A. tumefaciens*-mediated transformation) in tobacco leaf epidermal cells as fusions with the N-terminal (YN) or C-terminal (YC) fragment of YFP. As shown in Figure 1D, coexpression of XBAT35.2^{AA}-YN with ACD11-YC yielded a BiFC fluorescence signal that was observed primarily as punctate structures, indicating that the YFP fluorophore was reconstituted due to the interaction, or the very close proximity, of the two proteins. No fluorescence was observed when ACD11-YC or XBAT35.2^{AA}-YN was expressed with the corresponding empty vector.

IP assays were used to further confirm the interaction between XBAT35.2 and ACD11 in plant cells. Anti-HA agarose was used to isolate ACD11-YFP-HA from protein extracts prepared from transiently transformed tobacco leaves expressing ACD11-YFP-HA or coexpressing YFP-XBAT35.2^{AA}. In addition, protein extracts prepared from tobacco leaves singly expressing ACD11-YFP-HA or YFP-XBAT35.2^{AA} were mixed and used in IP assays. As shown in Figure 1E (lanes 2 and 3), ACD11-YFP-HA was able to interact with and pull down YFP-XBAT35.2^{AA}.

Glutathione *S*-transferase (GST) pull-down assays were carried out to provide support for the direct interaction between ACD11 and XBAT35.2. Purified recombinant Flag- and His-tagged ACD11 (Flag-His-ACD11) was used along with His-GST-tagged XBAT35.2 (His-GST-XBAT35.2) or the His-GST tag alone (negative control) in pull-down assays. His-GST-XBAT35.2 was able to pull down Flag-His-ACD11, compared with the control (His-GST), in multiple independent assays (Fig. 1F; Supplemental Fig. S2). No interaction was observed between Flag-His-ACD11 and another RING-type E3, Keep on Going [His-GST-KEG(RK)], in pull-down assays (Supplemental Fig. S2). Altogether, the results presented in Figure 1 provide strong evidence for XBAT35.2 interaction with ACD11.

XBAT35.2 Localizes Predominantly to the Golgi in Arabidopsis and Tobacco Cells

Previous intracellular localization studies using transiently transformed onion (*Allium cepa*) epidermal cells and Arabidopsis leaf protoplasts showed that XBAT35.1 was localized to the nucleus, while XBAT35.2 was distributed throughout the cytoplasm (Carvalho et al., 2012), which is consistent with the observations that XBAT35.2 lacks the amino acid sequence corresponding to the nuclear localization signal in XBAT35.1 (Fig. 2A). In this study, however, XBAT35.2 was observed predominantly in discrete punctate structures when expressed transiently in tobacco leaf epidermal cells (Fig. 1, A and B; Supplemental Fig. S1, B and C). Thus, to verify the subcellular location of the XBAT35 isoforms in Arabidopsis plants, we generated stable transgenic lines expressing YFP-HA-tagged versions of either isoform. Although we were able to recover transgenic plants, we did not retrieve plants with high enough levels of fluorescence attributable to XBAT35.2-YFP-HA to allow for microscopic analysis. Therefore, localization studies were carried out using XBAT35.2^{AA}-YFP-HA. As expected, XBAT35.1-YFP-HA localized to the nucleus of Arabidopsis root cells (Fig. 2B). In addition, XBAT35.2^{AA}-YFP-HA was detected predominantly in numerous discrete punctate structures and the cytoplasm in Arabidopsis root cells (Fig. 2C), consistent with its localization in transiently transformed tobacco cells (Fig. 1, A and B; Supplemental Fig. S1C).

Since XBAT35.2 was observed primarily at punctate structures within plant cells, we investigated the identity of these structures and did so with the presumption that, based on their size, number, and distribution, as well as their close association at times with the endoplasmic reticulum (ER; Supplemental Fig. S3A), they were Golgi. Consistent with this premise, the XBAT35.2^{AA}-YFP-HA-containing punctate structures in root epidermal and hair cells of stably transformed Arabidopsis seedlings were readily stained with *N*-(3-triethylammoniumpropyl)-4-(*p*-diethylaminophenyl-hexatrienyl)-pyridinium dibromide (FM4-64; Fig. 2, D and E), which is a well-known marker of the compartments of the endocytic pathway in plants, including Golgi (Bolte et al., 2004). Moreover, XBAT35.2-YFP-HA colocalized with the well-characterized Golgi marker protein Man49-CFP (consisting of mannosidase 49 linked to CFP; Nelson et al., 2007) in both transiently cotransformed tobacco leaf epidermal cells (Fig. 2F) and *N. tabacum* suspension-cultured cells (Fig. 2G). Colocalization was not observed, however, between XBAT35.2-YFP-HA and a peroxisomal marker protein (i.e. Cherry-PTS1;

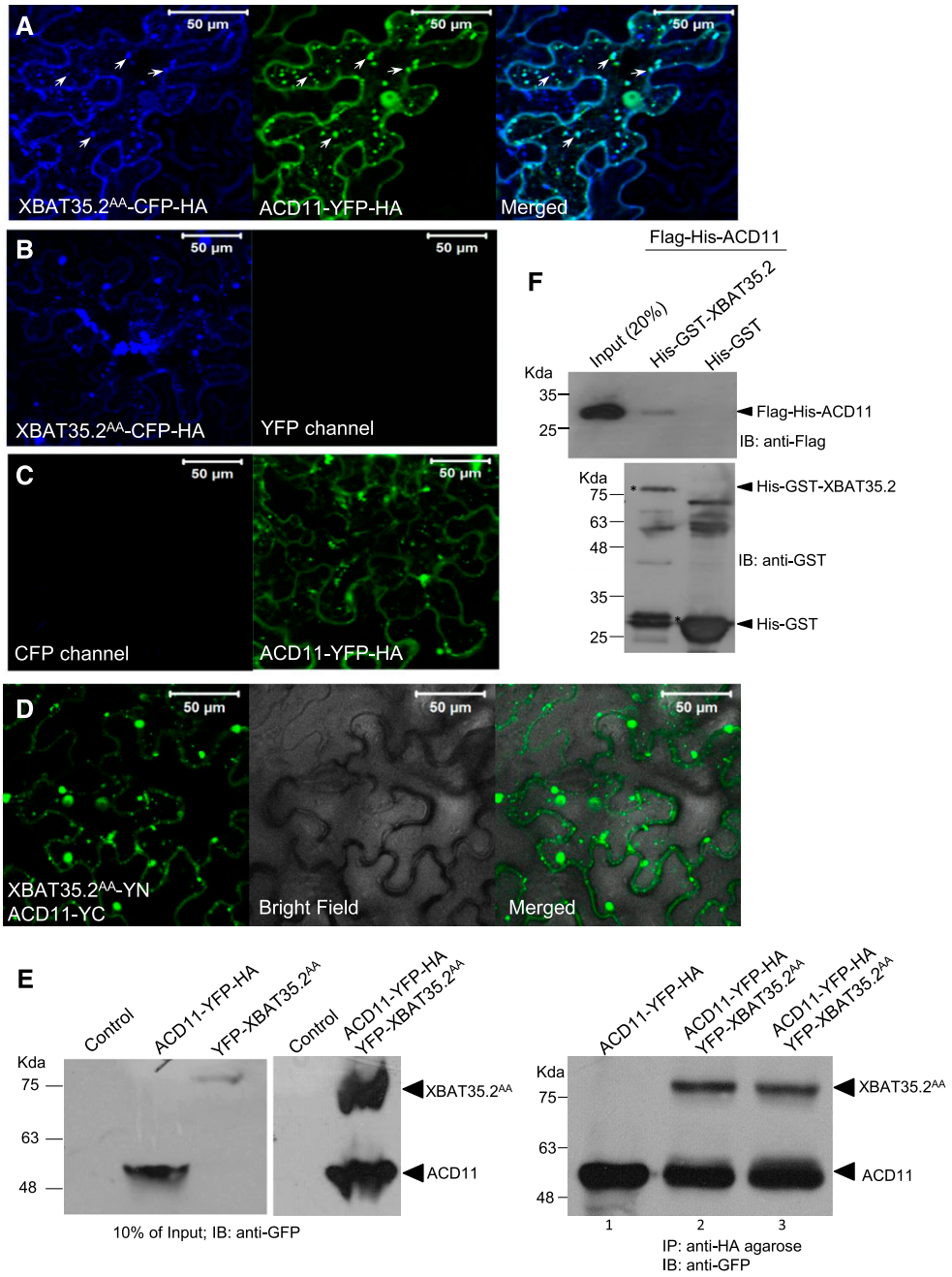

Figure 1. XBAT35.2 interacts with ACD11. A to C, Colocalization of XBAT35.2 with ACD11. XBAT35.2^{AA}-CFP-HA colocalizes with ACD11-YFP-HA (A) in transiently cotransformed tobacco leaf epidermal cells using agroinfiltration. Single transformations were used as controls to show no overlap between CFP and YFP channels (B and C). Left and middle micrographs show CFP and YFP fluorescence images, respectively, from a combined Z-stack series. The right micrograph in A shows the corresponding CFP and YFP merged image. Arrows in A highlight examples of the colocalization of XBAT35.2^{AA}-CFP-HA and ACD11-YFP-HA at punctate structures. D, BiFC analysis of XBAT35.2 and ACD11 in tobacco leaf epidermal cells. Fluorescence indicates interaction between XBAT35.2^{AA}-YN and ACD11-YC. E, ACD11 is able to pull down XBAT35.2 from plant protein extracts. Anti-HA agarose was used to immunoprecipitate (IP) ACD11-YFP-HA from protein extracts prepared from transiently transformed tobacco leaves expressing ACD11-YFP-HA alone (lane 1, right gel) or coexpressing ACD11-YFP-HA and YFP-XBAT35.2^{AA} (lane 2, right gel). Protein extracts prepared from separate tobacco leaves expressing ACD11-YFP-HA or YFP-XBAT35.2^{AA} also were mixed and used in an IP assay (lane 3, right gel). Immunoblot (IB) analysis using GFP antibody was used to detect both ACD11-YFP-HA and YFP-XBAT35.2^{AA}. IB analysis with anti-GFP was used to detect both ACD11-YFP-HA and YFP-XBAT35.2^{AA} in protein extracts prepared from (co)transiently transformed and untransformed tobacco leaves (control) and in IP assays (left and middle gels). F, GST pull-down assays using purified Flag-His-ACD11 and His-GST (control) or His-GST-XBAT35.2. GST-XBAT35.2 was able to pull down Flag-His-ACD11 (top gel) as shown by IB analysis with Flag antibodies. IB with GST antibodies was used to visualize His-GST and His-GST-XBAT35.2 used in each assay (bottom gel). Asterisks indicate the relevant bands.

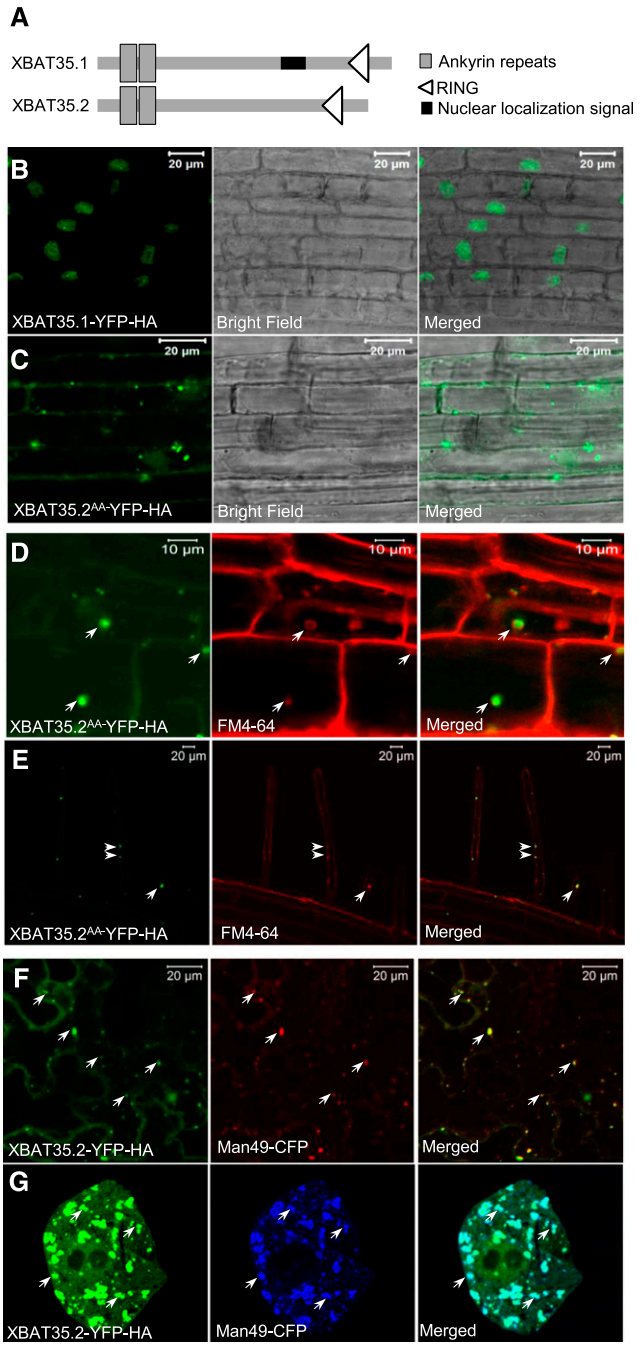

Figure 2. Subcellular localization of XBAT35.2. A, Schematic representation of XBAT35.1 and XBAT35.2. B and C, Localization of XBAT35.1-YFP-HA (B) and XBAT35.2^{AA}-YFP-HA (C) in root cells of transgenic Arabidopsis seedlings. Left micrographs show fluorescence images from a single optical section. Middle and right micrographs show the corresponding transmitted light (bright field) and merged images, respectively. D and E, Localization of XBAT35.2^{AA}-YFP-HA in root cells (D) and root hairs (E) of transgenic Arabidopsis seedlings treated for 30 min with FM4-64. Left micrographs show fluorescence images from a single optical section. Middle and right micrographs show the corresponding FM4-64 and merged images, respectively. Arrows highlight examples of the colocalization of XBAT35.2^{AA}-YFP-HA and FM4-64-stained punctate structures. F and G, Colocalization of XBAT35.2-YFP-HA with the Golgi protein marker Man49-CFP in transiently cotransformed tobacco leaf epidermal cells (F) and tobacco suspension-cultured cells (G). Arrows highlight examples of the colocalization of XBAT35.2^{AA}-YFP-HA and Man49-CFP in both cell types.

Ching et al., 2012) in *N. tabacum* suspension-cultured cells (Supplemental Fig. S3B), reconfirming that the XBAT35.2-containing structures were Golgi and not peroxisomes, which generally can resemble one another based on their appearance via confocal microscopy. Collectively, these results and those presented in Figure 1 indicate that XBAT35.2 localizes to the Golgi in plant cells.

XBAT35.2 Promotes the Proteasome-Dependent Degradation of ACD11 and Itself

XBAT35.2 is a functional RING-type E3 ligase capable of attaching ubiquitin to itself in in vitro ubiquitination assays (Supplemental Fig. S4; Carvalho et al., 2012). The interaction between XBAT35.2 and ACD11 suggests that the abundance of ACD11 may be regulated by the ubiquitin proteasome system. In in vitro ubiquitination assays containing yeast E1 and Arabidopsis E2 AtUBC8 (His-AtUBC8), recombinant XBAT35.2 (His-GST-XBAT35.2) was not found to attach ubiquitin to ACD11 (Flag-His-ACD11; Supplemental Fig. S4). A possible caveat of these results, however, is that Arabidopsis E3 ligases can utilize more than one of the 37 available E2 enzymes to facilitate ubiquitin conjugation to a substrate (Kraft et al., 2005); thus, the E2 used in this assay may not support XBAT35.2-mediated substrate ubiquitination. Also, PTM of the E3 ligase and/or substrate may be required to promote substrate ubiquitination (Hunter, 2007). To overcome these and other potential limitations, cell-free degradation assays (Wang et al., 2009) were employed to assess the stability of ACD11 in the presence of a functional (i.e. YFP-XBAT35.2) and a nonfunctional (i.e. YFP-XBAT35.2 ^{AA}) E3 ligase. Degradation assays were carried out using cell-free extracts prepared from transiently transformed tobacco leaves coexpressing ACD11-YFP-HA and YFP-XBAT35.2 or YFP-XBAT35.2 ^{AA}. In repeated trials and as shown in the representative blot in Figure 3A, the levels of ACD11-YFP-HA decreased gradually over time in the presence of YFP-XBAT35.2 while remaining fairly consistent in the presence of the nonfunctional YFP-XBAT35.2^{AA}. To determine if the observed turnover of ACD11 is proteasome dependent, MG132, a specific inhibitor of the 26S proteasome (Rock et al., 1994; Genschik et al., 1998), was added to the cell-free degradation assay. Despite the presence of YFP-XBAT35.2, the degradation of ACD11-YFP-HA was significantly slower in the presence of MG132 (Fig. 3A). To confirm the proteasome-dependent turnover of ACD11 in planta, seedlings stably expressing ACD11-GFP were treated with MG132. As shown in Figure 3B, the abundance of ACD11-GFP, based on its emission fluorescence, was

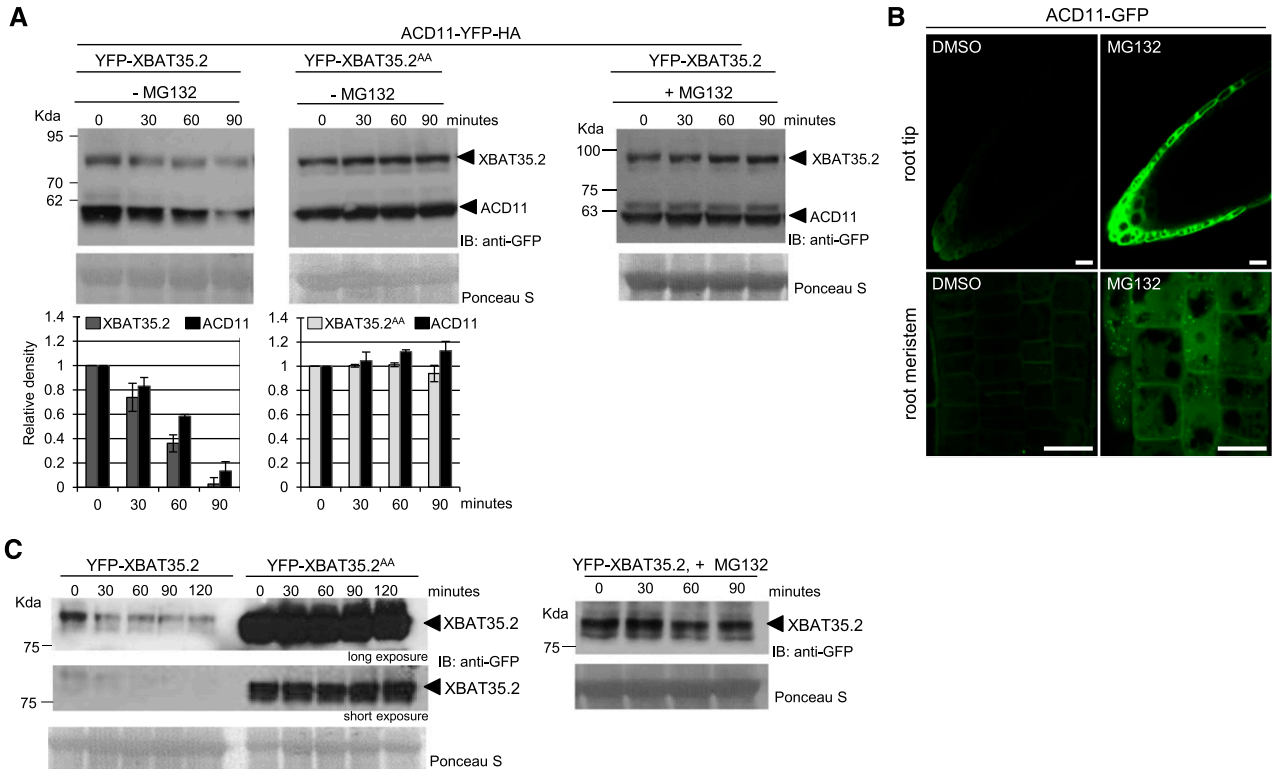

Figure 3. Proteasome-dependent turnover of ACD11 in the presence of XBAT35.2 and self-regulation of E3. A, Cell-free degradation assays using protein extracts prepared from transiently transformed tobacco leaves expressing ACD11-YFP-HA and YFP-XBAT35.2 or YFP-XBAT35.2^{AA} (RING mutant) treated with (+) or without (−) 50 μM MG132. The levels of ACD11, XBAT35.2, and XBAT35.2^{AA} were determined by immunoblot (IB) analysis using GFP antibodies at the indicated time points. Ponceau S staining shows protein loading. Graphs show average band density relative to the zero time point, as determined by ImageJ analysis, over three trials. Error bars represent SE. B, Five-day-old *35S:ACD11-GFP* transgenic Arabidopsis seedlings were treated overnight with dimethyl sulfoxide (DMSO; control) or 40 μM MG132. Identical imaging settings were used for DMSO and MG132 treatments. Bars = 20 μm. C, Cell-free degradation assays using protein extracts prepared from transiently transformed tobacco leaves expressing YFP-XBAT35.2, YFP-XBAT35.2^{AA}, or YFP-XBAT35.2 supplemented with (+) 50 μM MG132. The levels of YFP-XBAT35.2 and YFP-XBAT35.2^{AA} remaining at the indicated time points were determined by IB analysis using GFP antibodies. Ponceau S staining shows protein loading.

considerably greater in the presence of the proteasome inhibitor relative to DMSO-treated controls. Taken together, these results suggest that ACD11 is targeted to the proteasome for degradation and that XBAT35.2 is capable of promoting the turnover of ACD11.

Surprisingly, YFP-XBAT35.2 also was found to be unstable in cell-free degradation assays, whereas mutations within the RING domain of the E3 (i.e. YFP-XBAT35.2^{AA}) and treatment with MG132 resulted in its stabilization (Fig. 3, A and C). These results suggest that the abundance of XBAT35.2 is controlled by autoubiquitination, meaning that the E3 ligase may regulate its own stability.

Overexpression of XBAT35.2 Causes Cell Death in Tobacco, and a Functional RING Domain Is Required for Cell Death Induction

The interaction between XBAT35.2 with ACD11 (Fig. 1) and the finding that E3 can promote the degradation of ACD11 (Fig. 3) suggest a functional link between the two proteins and a role for XBAT35.2 in inducing cell death. *acd11* is a lethal lesion-mimic mutation that exhibits cell death and does not survive beyond the two- to four-leaf stage (Brodersen et al., 2002). Therefore, overexpression of XBAT35.2 may lead to a decrease in ACD11 abundance and possibly trigger cell death. To this end, *A. tumefaciens*-mediated transient transformation was used to determine if XBAT35.2 also was able to produce a cell death phenotype in tobacco leaves. Seventy-two hours postinfiltration, expression of XBAT35.2-YFP-HA was found to induce cell death, which coincided with the area where the *A. tumefaciens*-containing infiltration solution spread throughout the leaf (Fig. 4). Unlike XBAT35.2, transient expression of XBAT35.1-YFP-HA did not induce cell death in tobacco leaves (Fig. 4A). In addition, cell death was not observed following transient expression of the nonfunctional E3 ligase, XBAT35.2^{AA}-YFP-HA (Fig. 4B). The inability of XBAT35.1 and XBAT35.2^{AA} to induce cell death is not due to a lack of protein expression, since, as demonstrated via immunoblot analysis, XBAT35.1-YFP-HA

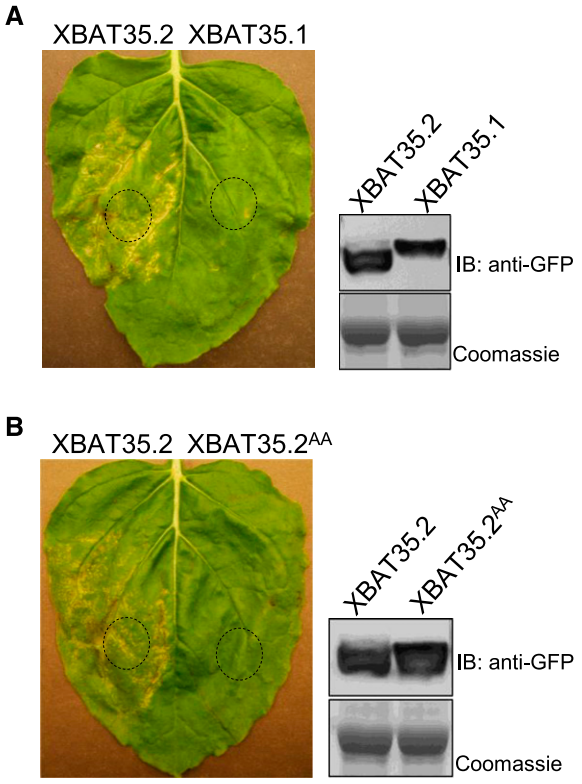

Figure 4. XBAT35.2 overexpression leads to cell death in tobacco leaves. Tobacco leaf epidermal cells were transiently transformed with agrobacteria carrying constructs for the expression of XBAT35.1-YFP-HA (A), XBAT35.2-YFP-HA (A and B), or nonfunctional XBAT35.2^{AA}-YFP-HA (B). Photographs were taken 72 h after infiltration. Circles indicate sites of infiltration. The expression of each transgene was detected by immunoblot (IB) analysis with GFP antibodies (gels at right).

and XBAT35.2^{AA}-YFP-HA were detected in the *A. tumefaciens*-infiltrated tissue (Fig. 4).

XBAT35 Is Required to Maintain Resistance to *Pseudomonas syringae* pv *tomato* DC3000

The ability of XBAT35.2 to interact with and promote the turnover of ACD11 and to induce cell death points to a possible involvement in plant defense. To determine a potential role of *XBAT35.2* during pathogen infection, we used *xbat35-1* plants lacking the expression of both *XBAT35* isoforms (Fig. 5A) and two independent transgenic lines (*35S:HA-XBAT35.2A* and *35S:HA-XBAT35.2B*) expressing HA-XBAT35.2 (Fig. 5B). Western-blot analysis was used to confirm the presence of HA-XBAT35.2 in both transgenic lines, and the level of transgenic protein detected in *35S:HA-XBAT35.2A* was lower compared with that observed for *35S:HA-XBAT35.2B* plants (Fig. 5B). The growth and development of *xbat35-1* and *35S:HA-XBAT35.2A/B* plants were similar to those of wild-type plants under standard growth conditions and, unlike *ACD11* loss-of-function mutants, did not show any obvious cell death phenotypes (Fig. 5C; Supplemental Fig. S5). When challenged with virulent *Pst* DC3000, *xbat35-1* plants exhibited increased susceptibility and had higher titers of bacteria compared with wild-type plants (Fig. 5, C and D). The transgenic line *35S:HA-XBAT35.2B* displayed reduced disease symptoms after *Pst* DC3000 infection and, consequently, lower bacterial load compared with the wild type (Fig. 5, C and D). In contrast, *35S:HA-XBAT35.2A*, with lower levels of HA-XBAT35.2 compared with *35S:HA-XBAT35.2B*, displayed disease symptoms and bacterial titers similar to those of the wild type (Fig. 5, C and D).

Next, we quantified the relative transcript levels of *Pathogenesis-Related Protein1* (*PR1*), a defense-related gene, in response to *Pst* DC3000 infection. The level of *PR1* expression in *xbat35-1* plants at 48 h post inoculation (hpi) was not significantly different from that of the wild type (Fig. 5E). However, overexpression of *XBAT35.2* resulted in enhanced expression of *PR1*, correlating with the observed reduced disease symptoms (Fig. 5E).

Stabilization of XBAT35.2 following Inoculation with Virulent and Avirulent Strains of *Pst* DC3000

XBAT35.2 appeared to promote its own proteasome-dependent turnover in cell-free degradation assays (Fig. 3, A and C), suggesting that the activity of the E3 ligase is controlled by self-regulation and, as such, may be used to maintain low levels of the E3 ligase in the absence of pathogen. Therefore, it is possible that pathogen infection promotes the accumulation of XBAT35.2 so that the E3 ligase then targets specific substrates to mediate defense responses such as cell death. To determine if XBAT35.2 is stabilized upon pathogen infection, transgenic Arabidopsis seedlings stably expressing HA-XBAT35.2 (*35S:HA-XBAT35.2B*) were either mock treated or inoculated with *Pst* DC3000, and the abundance of the E3 ligase was assessed by western-blot analysis with HA antibodies. As shown in Figure 6A, the abundance of XBAT35.2 was found to increase substantially with *Pst* DC3000 (12 hpi) compared with mock-treated plants. The analysis was expanded to determine if XBAT35.2 stabilization also occurs in response to inoculation with avirulent *Pst* DC3000 expressing the bacterial effectors AvrRPT2 and AvrRPM1. Indeed, the level of HA-XBAT35.2 did increase upon exposure to both avirulent strains of the pathogen (Fig. 6A).

To provide further evidence for pathogen-induced XBAT35.2 stabilization, the level of ubiquitinated XBAT35.2 in the presence and absence of pathogen was assessed. As expected, HA-XBAT35.2 isolated from mock-treated transgenic Arabidopsis seedlings was highly ubiquitinated, indicating the proteasome-dependent degradation of the protein in the absence of pathogen (Fig. 6B). In contrast, the level of ubiquitinated HA-XBAT35.2 was reduced greatly following inoculation with both virulent and avirulent strains of the pathogen (Fig. 6B), suggesting a significant decrease in ubiquitin-dependent proteolysis.

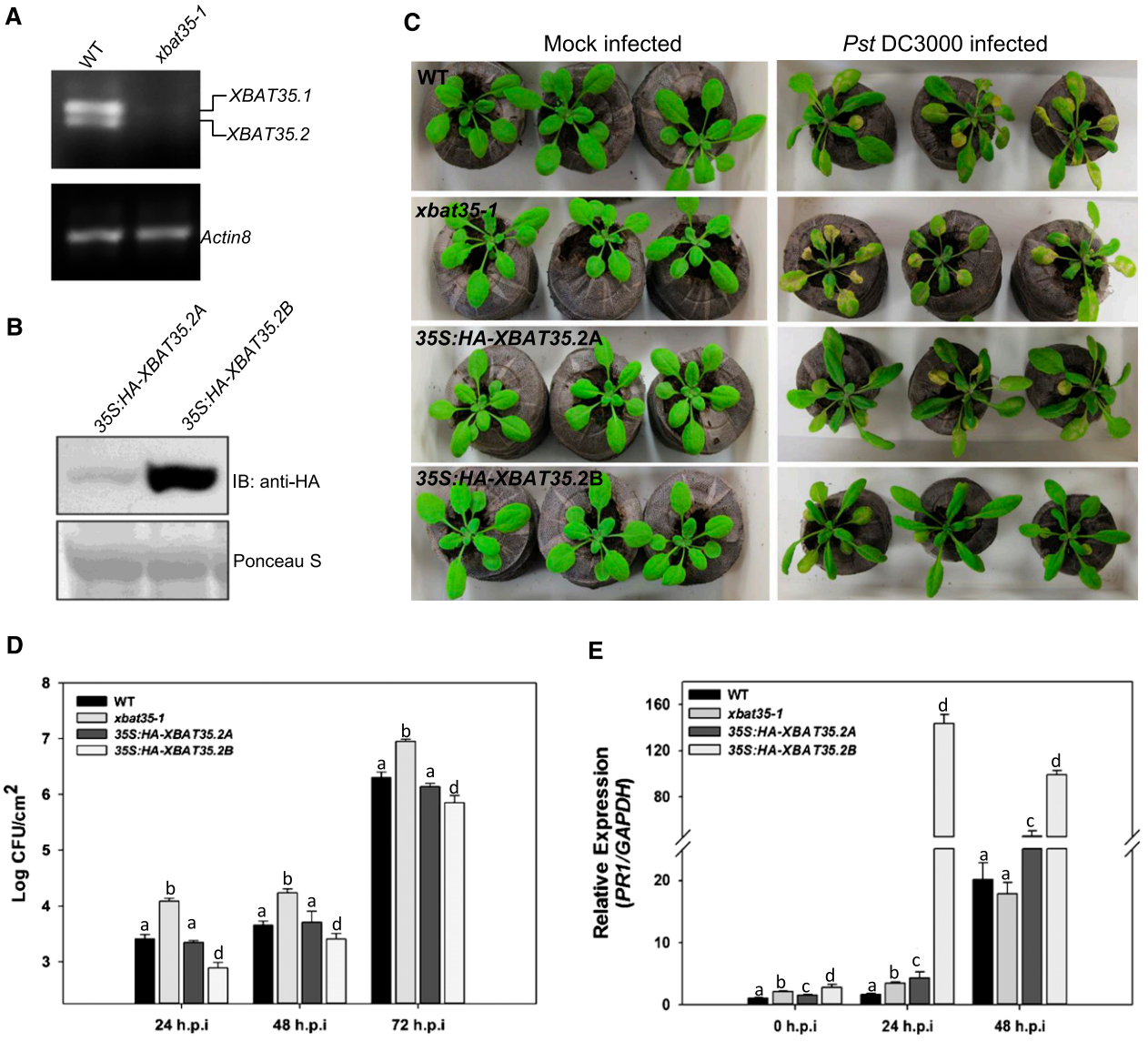

Figure 5. XBAT35.2 is involved in defense against *Pseudomonas syringae* pv *tomato* (*Pst*) DC300. A, Reverse transcription-PCR showing levels of *XBAT35.1* and *XBAT35.2* transcript in wild-type (WT) and *xbat35-1* mutant seedlings. B, Western-blot analysis showing protein levels of HA-XBAT35.2 in two independent Arabidopsis transgenic lines, *35S:HA-XBAT35.2A* and *35S:HA-XBAT35.2B*. Ponceau S staining shows protein loading. C, Representative images showing phenotypes of 5-week-old wild-type, *xbat35-1*, *35S:HA-XBAT35.2A*, and *35S:HA-XBAT35.2B* plants following mock and *Pst* DC3000 infection. D, Growth of virulent *Pst* DC3000 in the wild type, *xbat35-1*, *35S:HA-XBAT35.2A*, and *35S:HA-XBAT35.2B*. Plants were inoculated with *Pst* DC3000 (10^{-8} colony-forming units [cfu] mL^{-1}), and bacterial growth was determined at the indicated time points. Values represent means ± SD from three separate trials with six to eight replicates in each trial. E, Transcript levels of *PR1* in wild-type, *xbat35-1*, *35S:HA-XBAT35.2A*, and *35S:HA-XBAT35.2B* plants before and after *Pst* DC3000 infection. Total RNA was extracted from leaf tissues sampled 0, 24, and 48 hpi. Transcript levels were normalized to the expression of glyceraldehyde 3-phosphate dehydrogenase (*GAPDH*) in the same samples. Transcript levels were expressed relative to the normalized transcript levels of wild-type plants. Values represent means ± SD from two independent experiments. For D and E, the letter a indicates no significant difference ($P > 0.05$) compared with the wild type and letters b to d indicate significant differences ($P < 0.05$) compared with the wild type. Statistical analysis was performed using Student's *t* test.

Increased Ubiquitination and Proteasome-Dependent Turnover of ACD11 following Inoculation with Virulent and Avirulent Strains of *Pst* DC3000

Based on the results presented in Figure 6, the pathogen-induced stabilization of the E3 ligase XBAT35.2 was hypothesized to target substrates for ubiquitination and subsequent degradation, which would facilitate the activation of defense responses. Hence, the increase in XBAT35.2 abundance after pathogen infection should correlate with a decrease in the levels of the potential substrate ACD11. To determine if this was the case, Arabidopsis seedlings expressing ACD11-GFP were mock treated or inoculated with virulent and avirulent

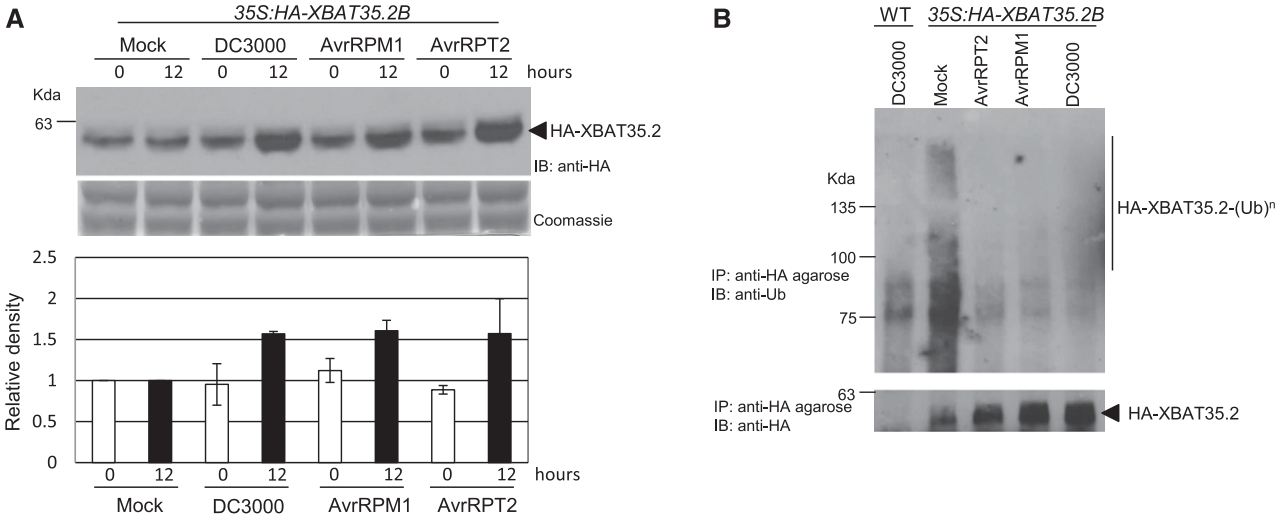

Figure 6. Accumulation of XBAT35.2 after pathogen infection. A, Increase in XBAT35.2 levels following pathogen infection. Two-week-old *35S:HA-XBAT35.2B* transgenic Arabidopsis seedlings were mock treated or infected for 12 h with the indicated *P. syringae* pathogen. The levels of HA-XBAT35.2 were determined at 0 and 12 hpi by immunoblot (IB) analysis using HA antibodies. Coomassie Blue staining of a duplicate gel shows protein loading. The graph below shows average band density relative to mock treatment, as determined by ImageJ analysis, over two trials. Error bars represent SE. B, Decrease in levels of ubiquitinated XBAT35.2 after pathogen infection. HA-XBAT35.2 was immunoprecipitated (IP) using anti-HA agarose from protein extracts prepared from 2-week-old wild-type (WT) or *35S:HA-XBAT35.2B* transgenic Arabidopsis seedlings mock treated or infected for 12 hpi with the indicated *P. syringae* pathogen. Immunoprecipitated proteins were subjected to IB analysis using ubiquitin (Ub; top gel) or HA (bottom gel) antibodies. The high-molecular-mass smear observed with ubiquitin antibodies indicates the ubiquitinated forms of HA-XBAT35.2.

(AvrRPT2 and AvrRPM1) strains of *Pst* DC3000, and the abundance of ACD11 was assessed by western-blot analysis with GFP antibody. The level of ACD11 was found to decrease drastically following inoculation with virulent *Pst* DC3000 and avirulent *Pst* DC3000 AvrRPM1 compared with mock-treated plants (Fig. 7A). In contrast, only a slight reduction in ACD11 abundance was observed following inoculation with *Pst* DC3000 AvrRPT2 (Fig. 7A).

To provide further evidence for the pathogen-induced degradation of ACD11, the level of ACD11 ubiquitination was determined following mock and *Pst* DC3000 AvrRPM1 inoculation. The level of ubiquitinated ACD11-GFP isolated from *Pst* DC3000 AvrRPM1-treated plants was significantly higher than that isolated from mock-treated plants (Fig. 7B) and was further increased substantially by MG132 treatment (Fig. 7B). Together, these results suggest the pathogen-induced ubiquitin-dependent proteasomal degradation of ACD11.

DISCUSSION

The function of both alternatively spliced isoforms of *XBAT35*, *XBAT35.1* and *XBAT35.2*, was linked previously to the negative regulation of ethylene responses, specifically apical hook curvature (Carvalho et al., 2012). Here, we demonstrate a new role for XBAT35.2 in cell death induction and defense against pathogens. This characterization of XBAT35.2 is supported by the finding that the E3 ligase interacts with and promotes the degradation of ACD11 (Figs. 1 and 3), which is known to be involved in defense against pathogens (Brodersen et al., 2002). ACD11 is ubiquitinated in vivo, and protein abundance increases in plant cells treated with proteasome inhibitors, providing further evidence for ubiquitin-dependent proteolysis (Figs. 3 and 7). Importantly, the abundance of XBAT35.2 was increased greatly in response to pathogen infection, which correlates with a pathogen-induced reduction in ACD11 levels (Figs. 6 and 7). In support of the observed changes in abundance, pathogen infection leads to a decrease in XBAT35.2 ubiquitination and a concomitant increase in the level of ubiquitinated ACD11 (Figs. 6 and 7).

In this study, XBAT35.2 was found to reside primarily at the Golgi (Fig. 2), which seemingly is in contrast to a recent report proposing that this protein is localized exclusively to the cytoplasm (Carvalho et al., 2012). One possible reason for this apparent dissimilarity in the localization of XBAT35.2 could be the difference in experimental systems employed in these two studies. That is, in this study, stably transformed Arabidopsis plants, as well as transiently transformed tobacco leaves and suspension cells, were employed, while the previous report made use of transiently transformed isolated Arabidopsis protoplasts and onion cells (Carvalho et al., 2012). The difference in localization may not be attributed to the positioning of the tag utilized by either study, since the fluorescent protein was similarly linked to the C terminus of XBAT35.2. Regardless of the reason, the subcellular

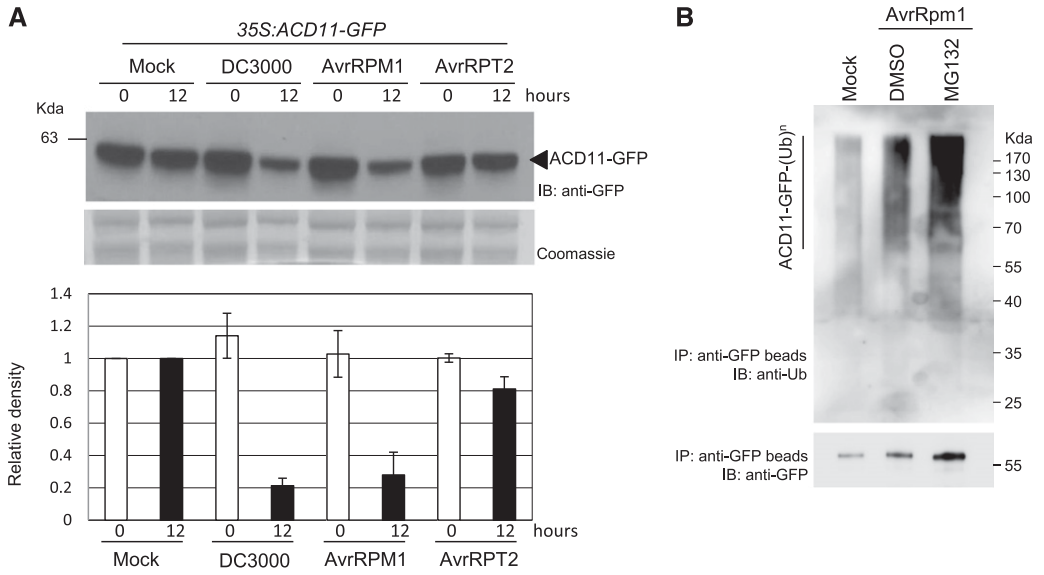

Figure 7. Ubiquitination and proteasome-dependent degradation of ACD11 after pathogen infection. A, Decrease in ACD11 abundance postinoculation. Two-week-old *35S:ACD11-GFP* transgenic Arabidopsis seedlings were mock treated or infected for 12 h with the indicated *P. syringae* pathogen. The levels of ACD11-GFP were determined 0 and 12 hpi by immunoblot (IB) analysis using GFP antibodies (top). Coomassie Blue staining of a duplicate gel shows protein loading. The graph at bottom shows average band density relative to mock-treated samples, as determined by ImageJ analysis, over three trials. Error bars represent SE. B, Increase in levels of ubiquitinated ACD11-GFP after pathogen infection. Rosette leaves of 6-week-old *35S:ACD11-GFP* plants were infiltrated without (Mock) or with *Pst* DC3000 AvrRpm1. Inoculated leaf discs were collected 1 hpi and treated with DMSO (control) or 40 μM MG132. ACD11-GFP was immunoprecipitated (IP) using anti-GFP beads and analyzed by IB analysis using ubiquitin (Ub) antibodies (top gel). The high-molecular-mass smear observed with ubiquitin antibodies indicates the ubiquitinated forms of ACD11-GFP. The immunoblot was stripped and reprobed with GFP antibodies (bottom gel).

localization of XBAT35.2 correlates well with that of another identified interacting protein, AtPRA1.F4 (Braun et al., 2011). The AtPRA1.Fs (AtPRA1.F1–AtPRA1.F4) are localized predominantly to Golgi and endosomal compartments (Kamei et al., 2008). Similar to XBAT35.2, the localization of AtPRA1.F1 was confirmed by colocalization with the endocytic tracer FM4-64 and the Golgi fluorescence-tagged organelle marker Man49:mCherry (Kamei et al., 2008). Mammalian PRA1 (also known as Yip3 or prenylin) and the yeast ortholog, Yip3p, also are localized to the Golgi (Abdul-Ghani et al., 2001; Geng et al., 2005). Interestingly, ACD11 also was shown to interact with PRA1.F2 and PRA1.F3 in Y2H assays (Petersen et al., 2009; Braun et al., 2011). XBAT35.2, ACD11, and one or more of the four AtPRA1.Fs may participate in the formation of a protein complex, wherein ACD11 interacts directly with XBAT35.2 or an AtPRA1.F mediates the interaction between ACD11 and XBAT35.2. In plants, PRA1s have been linked to vesicle trafficking and fusion (Heo et al., 2010; Lee et al., 2011). However, similar to ACD11 and XBAT35.2, the interacting AtPRA1.Fs may be involved in plant immunity as components of the vesicle-trafficking system are actively engage in mounting defense against pathogens (Frei dit Frey and Robatzek, 2009; Nomura et al., 2011, Pecenková et al., 2011; Stegmann et al., 2012). Although the significance of the interaction between AtPRA1.Fs, XBAT35.2, and ACD11 needs to be explored, the interaction provides further support for the Golgi localization of XBAT35.2.

XBAT35.2 and other members of the RING-ankyrin E3 ligase subfamily are structurally related to rice XB3, which similarly induces cell death when transiently overexpressed in tobacco leaves in the absence of pathogen (Wang et al., 2006; Huang et al., 2013). Other XB3-related proteins, such as XBAT31, XBOS31 (rice), and XBCT31 (*Citrus sinensis*), also were found to elicit cell death when transiently expressed in tobacco leaves (Huang et al., 2013), suggesting a conserved function among the members of the subfamily of RING-type E3 ligases. On the other hand, XBAT32, XBCT32, and XBAT35.1 do not trigger cell death when overexpressed in tobacco cells, indicating variations in function (Huang et al., 2013; this study). However, this does not preclude a role for these RING-ankyrin proteins in plant immunity. Whether cell death triggered by other XB3-related proteins, such as XBAT31, also is involved in disease resistance remains to be determined. The role of XBAT35.2 in eliciting cell death may be linked to its previously described function in regulating ethylene responses (Carvalho et al., 2012). Ethylene signaling is involved in regulating programmed cell death during development and defense against pathogens (Huysmans et al., 2017). In Arabidopsis, ethylene signaling is considered a positive regulator of pathogen-induced cell death (Bouchez et al., 2007; Liu et al., 2008).

However, XBAT35.2 is thought to inhibit ethylene responses, suggesting that E3 does not facilitate the ethylene-dependent regulation of programmed cell death in disease.

The interaction between XBAT35.2 and ACD11 suggests a role for the RING-type E3 ligase in plant immunity. Plants lacking *ACD11* gene function do not survive beyond the seedling stage due to the activation of programmed cell death and the constitutive expression of defense-related genes, such as *PR1*, without prior exposure to pathogens (Brodersen et al., 2002). *xbat35-1* displays opposing phenotypes to *acd11*, including a lack of spontaneous cell death (Supplemental Fig. S5) and increased susceptibility to pathogens (Fig. 5), which indicates impairment in the activation of defense responses. On the other hand, overexpression of *XBAT35.2* induces cell death in tobacco cells and reduces the susceptibility to pathogens in transgenic Arabidopsis plants, which correlates with enhanced expression of *PR1*. The resistance of *XBAT35.2*-overexpressing transgenic plants to pathogen attack, as measured by bacterial growth, while significant, was not enhanced greatly compared with the wild type (Fig. 5). The level of susceptibility to pathogens correlates with the abundance of E3, where transgenic plants with higher levels of HA-XBAT35.2 (*35S:HA-XBAT35.2B*) display lower bacterial titer and greater expression of *PR1* (Fig. 5). Thus, resistance to pathogens may be enhanced further by increasing the level of *XBAT35.2* expression. However, we did not recover transgenic Arabidopsis plants with higher levels of XBAT35.2, despite the use of different plant transformation vectors that allow for the expression of various fusion proteins, including those with an appended YFP and/or HA tag. As observed for transiently transformed tobacco cells (Fig. 3), XBAT35.2 is capable of inducing cell death when overexpressed, and this deleterious effect may explain why we were unable to generate stable transgenic plants that express higher levels of the E3 ligase. A significant increase in XBAT35.2 abundance may result in the misregulation of ubiquitin ligase activity, allowing for substrate ubiquitination and subsequent degradation leading to cell death.

The results of this study suggest a functional link between XBAT35.2 and ACD11 whereby XBAT35.2 promotes the degradation of ACD11 to elicit cell death and assist in defense against pathogens. We showed that ACD11 is ubiquitinated and degraded by the 26S proteasome in plant cells (Figs. 3 and 7). We also provided evidence for XBAT35.2's interaction with ACD11 in planta and its involvement in promoting the turnover of ACD11 in cell-free degradation assays (Fig. 3). Furthermore, the level of ubiquitinated ACD11 increases and protein abundance decreases postinoculation, indicating pathogen-induced ubiquitin-dependent proteasomal degradation (Fig. 7). The notion that XBAT35.2 mediates the ubiquitin-dependent degradation of ACD11 correlates well with the phenotype of *xbat35-1* (Fig. 5), where, in the absence of XBAT35.2, the inability to efficiently promote the ubiquitination and subsequent degradation of ACD11 to effectively trigger cell death may hamper defense responses and increase susceptibility. Other E3 ligases also may target ACD11 for degradation, which would allow the plant to dampen the negative effects of the *XBAT35.2* mutation during pathogen attack. The similarity in phenotypes of the *acd11* null mutant, where programmed cell death pathway and defense-related genes are constitutively activated, and that of *XBAT35.2* overexpression, which elicits cell death and reduces susceptibility to pathogens (Fig. 5), also provides support for ACD11 as a potential substrate for XBAT35.2. The overexpression of XBAT35.2 would lead to more efficient degradation of ACD11 in response to pathogen perception, which may allow the plant to more effectively trigger cell death and initiate defense signaling pathways similar to those that are activated in the *acd11* null mutant.

Self-regulation is a mechanism used to modulate the activity of many RING-type E3 ligases (de Bie and Ciechanover, 2011; Berndsen and Wolberger, 2014). Similarly, XBAT35.2 was observed to conjugate ubiquitin to itself in in vitro assays (Supplemental Fig. S4) and promote its own proteasome-dependent degradation in cell-free degradation assays (Fig. 3). The reduction in the level of ubiquitinated XBAT35.2 and the accumulation of the E3 ligase observed postinoculation (Fig. 6) suggest that defense signaling initiated in response to pathogen infection may prohibit self-catalyzed ubiquitination. The phosphorylation of XBAT35.2 may be the underlying mechanism that switches the E3 ligase from autoubiquitination to substrate ubiquitination. The interplay between ubiquitination and phosphorylation is quite extensive, can occur at the level of the modifying enzymes and/or substrates, and each PTM is capable of antagonizing or promoting the functioning of the other (Hunter, 2007; Swaney et al., 2013). Phosphorylation of the E3 ligase can regulate function in different ways, such as activating the enzyme to allow for substrate ubiquitination, promoting self-ubiquitination to inhibit activity, or switching substrate specificity (Yang et al., 2006; Cheng et al., 2011; Dou et al., 2012). Phosphorylation of the substrate can promote ubiquitination via the creation of phosphodegrons, which are phosphorylated residues that allow for recognition by the E3 ligase (Hunter, 2007). Plant defense-related E3 ligases known to be phosphorylated include XB3, which is modified by Xa21, a receptor-like kinase involved in pathogen-associated molecular pattern-triggered immunity (Ronald et al., 1992; Song et al., 1995). The Plant U-Box-type (PUB) E3 ligases, PUB22 and PUB13, are both phosphorylated by BAK1, a signaling partner for the bacterial flagellin receptor Flagellin-Sensing2 (FLS2; Wang et al., 2006; Lu et al., 2011). However, the effect of phosphorylation on the activity of these E3 ligases is not known. Regardless, it is intriguing to postulate that pathogen perception triggers the phosphorylation (or possibly dephosphorylation) of XBAT35.2, which may then prohibit autoubiquitination, allowing the stabilization of the E3 ligase and promote substrate

ubiquitination. The need for PTMs, such as phosphorylation, to promote substrate ubiquitination may explain why recombinant XBAT35.2 was not able to conjugate ubiquitin to ACD11 in in vitro ubiquitination assays (Supplemental Fig. S4). Phosphorylation sites have been predicted and identified experimentally for XBAT35.2, indicating that E3 is a phosphoprotein (Durek et al., 2010; Engelsberger and Schulze, 2012). But how phosphorylation and possibly other types of PTMs, such as acetylation or nitrosylation, may regulate XBAT35.2 functioning remains an open question.

The self-regulation and pathogen-induced stabilization of XBAT35.2 lead us to propose a model where, in the absence of pathogen, autoubiquitination maintains low levels of the E3 ligase, allowing for the accumulation of substrate proteins. In the presence of pathogens, the stabilized XBAT35.2 would accumulate and mediate the proteasome-dependent degradation of substrates, such as ACD11, to promote defense responses. This regulatory mechanism is similar to that described for PUB22, where the perception of flg22, which activates FLS2-mediated defense signaling, results in the stabilization of the U-box-type E3 ligase (Zipfel et al., 2004; Stegmann et al., 2012). However, in contrast to XBAT35.2, the accumulation of PUB22 is thought to attenuate pathogen-initiated defense signaling (Stegmann et al., 2012). In addition to a decrease in ubiquitin-dependent proteolysis, an increase in *XBAT35.2* transcript levels may also contribute to the pathogen-induced accumulation of E3. The accumulation of XBAT35.2 is observed following inoculation with virulent (*Pst* DC3000) and both avirulent (*Pst* DC3000 AvrRPM1 and AvrRPT2) strains of the pathogen (Fig. 6). The decrease in ACD11 abundance was reduced greatly following inoculation with *Pst* DC3000 and *Pst* DC3000 AvrRPM1 but less so in response to *Pst* DC3000 AvrRPT2 infection (Fig. 7). This suggests that ACD11 may not be targeted for degradation as part of the response initiated to defend against *Pst* DC3000 AvrRPT2 and that ubiquitin-dependent proteolysis of ACD11 may be limited to responses to specific bacterial strains. XBAT35.2 may target other defense-related proteins to promote defense against *Pst* DC3000 AvrRPT2. In addition to identifying other ubiquitin substrates, it would be worth exploring the degree to which XBAT35.2 is involved in plant immunity by elucidating the requirement for the E3 ligase in defense against different types of pathogens with varying lifestyles.

MATERIALS AND METHODS

Cloning and Mutagenesis

Full-length *ACD11* (At2g34690) cDNAs were obtained from the Arabidopsis Biological Resource Center (Alonso et al., 2003). These cDNAs were amplified via PCR using Phusion polymerase (Finnzymes) to remove the stop codon. To obtain full-length cDNAs for *XBAT35* (At3g23280) isoforms, *XBAT35.1* and *XBAT35.2*, total RNA isolated from 10-d-old Arabidopsis (*Arabidopsis thaliana*) seedlings was used in reverse transcription-PCR to amplify the predicted open reading frames. TRI Reagent (Sigma-Aldrich) was used to isolate total RNA as per the manufacturer's instructions. For XBAT35.2^{AA}, the Phusion site-directed mutagenesis kit (Finnzymes) was used to make two point mutations, C426A and H428A, within the RING domain-encoding region of the cDNA. All cDNAs were introduced into the Gateway entry vector pDONR201 (Invitrogen) as per the manufacturer's instructions. Nucleotide sequences were confirmed by DNA sequencing (McGill University and Génome Québec Innovation Centre). For all primers used in this study, see Supplemental Table S1.

For plant transformations, cDNAs in the Gateway entry vector pDONR201 were recombined into the pEarleyGate plant transformation vectors using Gateway cloning (Invitrogen) to produce in-frame fusion proteins with the indicated tags under the control of the cauliflower mosaic virus 35S promoter (Earley et al., 2006). pEarleyGate101 plant transformation was used to produce in-frame fusions with the C-terminal YFP and HA tags (YFP-HA). The pEarleyGate102 plant transformation vector was used to generate C-terminal tagged CFP and HA (CFP-HA) fusions. pEarleyGate104 and pEarleyGate201 plant transformation vectors were used to produce in-frame fusions with the N-terminal YFP and HA tags, respectively. For BiFC assays, cDNAs in the Gateway entry vector pDONR201 were recombined into pEarleygate201-YN or pEarleygate202-YC plant transformation vector using Gateway cloning (Invitrogen). pEarleygate201-YN contains the N-terminal portion (amino acids 1–174) of enhanced YFP (eYFP) and an HA tag, and pEarleygate202-YC contains the C-terminal portion (amino acids 175–239) of eYFP and a FLAG tag. Both plant transformation vectors were a gift from Dr. Yuhai Cui's laboratory (Agriculture and Agri-Food Canada; Lu et al., 2010).

For the expression of recombinant proteins in bacterial cells, cDNAs in the Gateway entry vector pDONR201 were recombined into pDEST565 or a modified pDEST527 (Addgene plasmids 11520 and 11518, respectively; donated by Dominic Esposito, National Cancer Institute) to produce fusion proteins with His-GST tag and Flag-His tag, respectively. The modification of pDEST 527 was described previously (Liu and Stone, 2010). The expression plasmids containing *AtUBC8* and *KEG(RK)* (partial cDNA encoding for the RING and kinase domain of KEG) were described previously by Kraft et al. (2005) and Liu and Stone (2010), respectively.

Plant Material, Growth Conditions, and Transformation

Arabidopsis ecotype Columbia-0 wild-type, mutant, and transgenic seeds were surface sterilized with 50% (v/v) bleach and 0.1% (v/v) Triton X-100. After cold treatment at 4°C for 48 h, seeds were germinated and grown on solid 0.5× Murashige and Skoog (MS) medium containing 0.8% agar and 1% Suc under continuous light at 22°C. For plants grown in soil, 7-d-old seedlings were transferred from MS medium to soil and grown under photoperiodic cycles of 16 h of light and 8 h of dark at 22°C in a growth chamber. *xbat35-1* (Salk_104813) seeds were obtained from the Arabidopsis Biological Resource Center (Alonso et al., 2003).

Transgenic Arabidopsis plants were generated using the flower-dipping method (Clough and Bent, 1998). For transformations, pEarleyGate 201 or pEarleyGate101 with *XBAT35.1* or *XBAT35.2* full-length wild-type and mutated cDNAs was introduced into *Agrobacterium tumefaciens* strain GV3101. Homozygous ACD11-GFP transgenic lines are as described previously by Munch et al. (2015).

Transient Protein Expression in Tobacco

Five-week-old tobacco (*Nicotiana benthamiana*) plants used for transient protein expression were grown under a photoperiod of 16 h of light and 8 h of dark at 23°C. *A. tumefaciens* strain GV3101 transformed with the appropriate binary plasmids was grown and prepared for transient expression as described previously (Sparkes et al., 2006; Liu and Stone, 2013). Briefly, *A. tumefaciens* cultures were resuspended in infiltration solution (5 mg mL^{-1} D-Glc, 50 mM MES, 2 mM Na_3PO_4, and 0.1 mM acetosyringone) at an optical density at 600 nm of 0.8. For infiltration with multiple constructs, coexpression, colocalization, and BiFC assays, *A. tumefaciens* suspensions were mixed in equal ratios. *A. tumefaciens* suspension mixtures were infiltrated using a needleless syringe into leaves of 5-week-old tobacco plants. Forty-eight hours after infiltration, leaf samples were collected for microscopic imaging and/or protein extraction. For the analysis of cell death, leaves were photographed up to 72 h after infiltration.

Nicotiana tabacum Cell Cultures and Microprojectile Bombardment

N. tabacum 'Bright Yellow-2' suspension cell cultures were maintained and prepared for bombardment as described previously (Lingard et al., 2008). Transient

(co)transformations were performed, depending on the plasmid, with 0.5 to 3 μg of plasmid DNA precipitated onto gold microcarriers (Bio-Rad), along with the Biolistic PDS-1000/He particle delivery system (Bio-Rad). Bombarded cells were incubated for ~6 h to allow expression and sorting of the introduced gene products and to reduce potential negative effects of protein overexpression. Cells were then fixed in 4% (w/v) formaldehyde and analyzed via confocal microscopy.

Subcellular Localization

CFP-tagged organelle markers for Golgi (pBIN20/Man49-CFP) and ER (pBIN20/HDEL-CFP) were described previously (Nelson et al., 2007). pMDC32/Cherry-PTS1, consisting of the Cherry red fluorescent protein linked to a C-terminal type 1 peroxisomal targeting signal, has been described elsewhere (Ching et al., 2012). Constructs were introduced into tobacco leaves or suspension cell cultures as described above. For endosomal staining, the FM4-64 dye (Sigma-Aldrich) was dissolved in water at a final concentration of 4 mM. Seedlings were incubated with the dye at room temperature for 30 min prior to microscopic analysis.

Fluorescence Microscopy and Proteasome Inhibitor Treatment

Roots of 7-d-old transgenic Arabidopsis seedlings or pieces of infiltrated tobacco leaf discs excised 48 h after infiltration were imaged using a Zeiss LSM 510 META inverted confocal laser scanning microscope (Carl Zeiss MicroImaging) equipped with a 25× oil-immersion objective. For YFP fluorescence, an excitation wavelength of 514 nm was used, and emissions were collected between 530 and 600 nm. For fluorescence images, a series of Z-stack images were collected and then combined and processed using the Zeiss LSM Image Browser (Carl Zeiss MicroImaging). To delineate the outline of each cell, single slices of the fluorescence and bright-field images were merged. For proteasome inhibitor treatment, 5-d-old seedlings from a homozygous ACD11-GFP transgenic line (Munch et al., 2015) were incubated overnight with either DMSO (solvent) or 40 μM MG132 (Z-Leu-Leu-Leu-al). Confocal laser scanning microscopy images of transgenic seedlings were acquired using a Zeiss LSM 780 device as described (Munch et al., 2015), and images of cv Bright Yellow-2 cells were acquired using a Leica DM RBE (Leica Microsystems) microscope with a Leica 63× Plan Apochromat oil-immersion objective (Leica TCS SP2). Fluorophore emissions were collected sequentially in double-labeling experiments; single-labeling experiments exhibited no detectable crossover at the settings used for data collection. Confocal images were acquired as single optical sections and saved as 512- × 512-pixel digital images.

Protein Extraction, Immunoblot Analysis, and IP Assays

Total protein was extracted from infiltrated tobacco leaves or Arabidopsis tissue using extraction buffer (50 mM HEPES, pH 7.5, 5 mM EDTA, 5 mM EGTA, 10 mM Na_3VO_4, 10 mM NaF, 50 mM β-glycerophosphate, 10 mM DTT, 1 mM phenylmethylsulfonyl fluoride, 5% glycerol, and protease inhibitor cocktail [Sigma-Aldrich]).

For immunoblotting, samples were mixed in 6× SDS loading buffer (300 mM Tris-HCl, pH 6.8, 30% glycerol, 12% SDS, and 0.6% Bromophenol Blue), boiled for 5 min, and then separated on SDS-PAGE gels. After electrophoresis, proteins were electrotransferred to polyvinylidene fluoride membranes. After blocking for 1 h in TBST (50 mM Tris-HCl, pH 7.5, 150 mM NaCl, and 0.05% Tween 20) with 5% nonfat dry milk at room temperature, membranes were incubated with primary rabbit anti-GFP, mouse anti-HA, or mouse anti-ubiquitin antibodies (Sigma-Aldrich) to detect the YFP tag, HA tag, or ubiquitinated proteins, respectively. Following three washes with TBST, membranes were incubated with secondary horseradish peroxidase (HRP)-conjugated goat anti-rabbit or goat anti-mouse antibodies (Sigma-Aldrich). Antibodies were diluted 1:5,000 using TBST with 1% nonfat dry milk. After three washes with TBST, immunoreactants were visualized using an enhanced Lumi-Light Western Blotting Substrate kit (Thermo Scientific) following the manufacturer's instructions. To visualize protein loading, polyvinylidene fluoride membranes was stained with a Ponceau S (Sigma-Aldrich) solution or a duplicate SDS-PAGE gel stained with Coomassie Brilliant Blue G-250 (Bio-Rad) was prepared (Thacker et al., 2016).

IP assays with anti-HA agarose (EZview Red Anti-HA Affinity Gel; Sigma-Aldrich) were as described previously (Liu and Stone, 2010). Total protein extract was prepared from *A. tumefaciens*-infiltrated tobacco leaves or Arabidopsis wild-type or transgenic seedlings as described above. Bradford assays were used to determine protein concentration, and 800 μg of total protein was used for pull-down assays. Isolated proteins were analyzed by western-blot analysis as described above with primary HA antibodies or ubiquitin antibodies at 1:5,000 dilution (Sigma-Aldrich) and secondary HRP-conjugated goat anti-mouse antibodies (Sigma-Aldrich) at 1:5,000 dilution. IP with anti-GFP beads (μMACS GFP Isolation Kit; Miltenyi Biotec) and immunoblot analysis were performed as described previously (Munch et al., 2015). Immunoprecipitated proteins were analyzed by western-blot analysis using ubiquitin antibodies (Agrisera) at 1:2,000 dilution and secondary HRP-conjugated anti-rabbit antibodies at 1:10,000 dilution.

Protein Expression and Purification

XBAT35.2 and KEG(RK) were expressed as His-GST fusions, ACD11 was expressed as a Flag-His-tagged fusion, and Arabidopsis AtUBC8 was expressed as a His-tagged fusion protein. All proteins were expressed in *Escherichia coli* strain Rosetta (DE3) and purified using nickel-charged resin according to the manufacturer's protocols (Bio-Rad).

GST Pull-Down Assays

Glutathione Sepharose 4B (GST beads) was prepared according to the manufacturer's instructions (GE Healthcare). GST beads were incubated for 45 min at 4°C in binding buffer (50 mM Tris-HCl, pH 7.5, 100 mM NaCl, and protease inhibitor cocktail [Sigma-Aldrich]) with purified His-GST-XBAT35.2, His-GST-KEG(RK) (control), or His-GST (control). Beads were then washed three times with wash buffer (50 mM Tris-HCl, pH 7.5, 100 mM NaCl, 0.05% Triton X-100, and protease inhibitor cocktail). Bead-bound His-GST and His-GST fusion proteins were then incubated for 45 min at 4°C in binding buffer with purified Flag-His-ACD11. Beads were then washed three times with wash buffer, and proteins were eluted by resuspending and boiling beads in 50 μL of 1× SDS loading buffer, separated by SDS-PAGE, followed by immunoblot analysis with Flag antibodies to detect Flag-His-FDH and with GST antibodies to detect His-GST-XBAT35.2, His-GST-KEG(RK), and His-GST.

In Vitro Ubiquitination Assays

Assays were performed as described previously (Stone et al., 2006). Briefly, 30-μL reactions containing 50 mM Tris-HCl, pH 7.5, 10 mM $MgCl_2$, 0.05 mM $ZnCl_2$, 1 mM ATP, 0.2 mM DTT, 10 mM phosphocreatine, 0.1 unit of creatine kinase (Sigma-Aldrich), 50 ng of yeast E1 (BostonBiochem), 250 ng of purified E2 His-AtUBC8, 300 or 600 ng of purified His-GST-XBAT35.2, 300 ng of Flag-His-ACD11, and 2 μg of ubiquitin (BostonBiochem) were incubated at 30°C for 2 h. Reactions were stopped by adding SDS sample buffer (125 mM Tris-HCl, pH 6.8, 20% glycerin, 4% SDS, and 10% β-mercaptoethanol) and resolved by SDS-PAGE followed by immunoblotting using GST (1:5,000 dilution; Sigma-Aldrich) or Flag (1:5,000 dilution; Sigma-Aldrich) antibodies.

Cell-Free Degradation Assays

Cell free degradation assays were carried out as described previously (Wang et al., 2009). Briefly, total protein extracts were prepared from *A. tumefaciens*-infiltrated tobacco leaves expressing ACD11-HA-YFP and XBAT35.2-YFP or XBAT35.2^{AA}-YFP. $MgCl_2$ (10 mM) and ATP (10 mM) were added to the reaction prior to incubation at 30°C, and the total reaction volume was adjusted to 120 μL with extraction buffer. For proteasome inhibitor treatments, 50 μM MG132 (Sigma-Aldrich) was added to the reaction 30 min prior to incubation at 30°C. A total of 30 μL of the reaction mixture was taken at the indicated time points, and 5 μL of 6× SDS loading buffer was added to stop the reaction. ACD11 and XBAT35.2 protein levels were determined by western-bolt analysis using HA or GFP antibodies (Sigma-Aldrich) as described above.

Pathogen Infection and Bacterial Growth Assay

Virulent *Pseudomonas syringae* pv *tomato* DC3000 and avirulent *Pst* DC3000 harboring AvrRpt2 or AvrRpm1 were used as bacterial strains. *Pst* DC3000 was grown on medium supplemented with rifampicin (100 μg mL^{-1}), and *Pst* DC3000 AvrRpt2 and *Pst* DC3000 AvrRpm1 (Dr. S-Y He, Michigan State University) were grown on medium supplemented with rifampicin (100 μg mL^{-1}) and kanamycin (25 μg mL^{-1}).

Plant inoculation and bacterial growth in plant apoplasts were determined as described by Zipfel et al. (2004). In brief, *Pst* DC3000 was cultured in King's B

medium supplemented with rifampicin (25 μg mL^{-1}) at 28°C until OD_{600} of 0.8. Bacterial cells were collected by centrifugation and resuspended in sterile water containing 0.02% Silwet L-77 (Lehle Seeds) to the final concentration of 10^8 cfu mL^{-1}. Plants (4–5 weeks old) were sprayed with bacterial suspension and kept under high humidity for disease development. For syringe inoculation, bacterial cultures were grown in King's B medium and resuspended in sterile water to a final concentration of 10^5 cfu mL^{-1}. The bacterial suspension was pressure infiltrated into the abaxial surface of leaves with a needleless syringe. For quantifying bacterial growth, leaves were excised 0, 24, and 48 hpi, surface sterilized with ethanol (75%, v/v), and rinsed with sterile water. Samples were prepared by pooling two leaf discs (0.5 cm^2) and ground in sterile water in a microfuge tube. The ground tissues were serially diluted and plated on King's B medium containing rifampicin (25 μg mL^{-1}). The plates were incubated at 28°C, and colonies were counted after 48 h. For *Pst* DC3000-induced gene expression, plants were sprayed with bacterial suspension (10^8 cfu mL^{-1}), and leaf tissues were frozen in liquid nitrogen at the time points indicated.

For seedling inoculation, 2-week-old Arabidopsis wild-type and transgenic seedlings were infected using the flood inoculation methods described by Ishiga et al. (2011). Briefly, bacterial strains grown on Luria-Bertani medium with the appropriate antibiotics were suspended in sterile water containing 0.025% Silwet L-77 (Lehle Seeds) to a final concentration of 5.7×10^7 cfu mL^{-1}. Seedlings grown on solid MS medium were immersed in the bacterial suspensions for 3 min at room temperature. The bacterial suspension was removed, and seedlings were placed under continuous light at 22°C. Seedlings were collected immediately (0 hpi) and at 12 hpi and used to prepare protein extracts.

For MG132 treatment following inoculation, rosette leaves of 6-week-old plants were syringe infiltrated with *Pst* DC3000 AvrRpm1 (OD = 0.2). One hour post infection, 25 to 27 leaf discs were harvested from the infected leaves and incubated in either DMSO or 40 μM MG132, subjected to vacuum infiltration, and remained incubated in the same solution for 3 h.

Quantitative Real-Time PCR

Total RNA was extracted from freeze-dried leaf tissues using a monophasic extraction method (Chomczynski and Sacchi, 1987). Reverse transcription was performed with 2 μg of total RNA using Quantiscript RTase (Qiagen). Relative transcript levels were assayed by real-time PCR using gene-specific primers (Supplemental Table S1) on the StepOnePlus Real-Time PCR system (Applied Biosystems) using SYBR Green reagent (Applied Biosystems). To determine the relative expression levels, the amount of target gene was normalized over the abundance of constitutive glyceraldehyde 3-phosphate dehydrogenase as an endogenous control. Primers (Supplemental Table S1) were generated using the Roche Universal Probe Library assay design center.

Accession Numbers

Sequence data from this article can be found in the GenBank/EMBL data libraries under accession numbers ACD11: AT2G34690; XBAT35: AT3G23280.

Supplemental Data

The following supplemental materials are available.

Supplemental Figure S1. Localization of XBAT35 isoforms and ACD11.

Supplemental Figure S2. GST pull-down assays.

Supplemental Figure S3. Coexpression of XBAT35.2-YFP-HA and ER or peroxisome protein markers.

Supplemental Figure S4. In vitro ubiquitination assays.

Supplemental Figure S5. The growth of *xbat35-1* is similar to that of wild-type plants.

Supplemental Table S1. Nucleotide sequences of primers used in this study.

ACKNOWLEDGMENTS

We thank Dr. Zhenyu Cheng (Dalhousie University) for reading the article and providing valuable feedback.

Received August 8, 2017; accepted September 23, 2017; published September 26, 2017.

LITERATURE CITED

Abdul-Ghani M, Gougeon PY, Prosser DC, Da-Silva LF, Ngsee JK (2001) PRA isoforms are targeted to distinct membrane compartments. J Biol Chem **276:** 6225–6233

Alonso JM, Stepanova AN, Leisse TJ, Kim CJ, Chen H, Shinn P, Stevenson DK, Zimmerman J, Barajas P, Cheuk R, et al (2003) Genome-wide insertional mutagenesis of *Arabidopsis thaliana*. Science **301:** 653–657

Berndsen CE, Wolberger C (2014) New insights into ubiquitin E3 ligase mechanism. Nat Struct Mol Biol **21:** 301–307

Bolte S, Talbot C, Boutte Y, Catrice O, Read ND, Satiat-Jeunemaitre B (2004) FM-dyes as experimental probes for dissecting vesicle trafficking in living plant cells. J Microsc **214:** 159–173

Bouchez O, Huard C, Lorrain S, Roby D, Balagué C (2007) Ethylene is one of the key elements for cell death and defense response control in the Arabidopsis lesion mimic mutant *vad1*. Plant Physiol **145:** 465–477

Braun P, Carvunis AR, Charloteaux B, Dreze M, Ecker JR, Hill DE, Roth FP, Vidal M, Galli M, Balumuri P, et al (2011) Evidence for network evolution in an Arabidopsis interactome map. Science **333:** 601–607

Brodersen P, Petersen M, Pike HM, Olszak B, Skov S, Odum N, Jørgensen LB, Brown RE, Mundy J (2002) Knockout of Arabidopsis accelerated-cell-death11 encoding a sphingosine transfer protein causes activation of programmed cell death and defense. Genes Dev **16:** 490–502

Carter S, Bischof O, Dejean A, Vousden KH (2007) C-terminal modifications regulate MDM2 dissociation and nuclear export of p53. Nat Cell Biol **9:** 428–435

Carvalho SD, Saraiva R, Maia TM, Abreu IA, Duque P (2012) XBAT35, a novel Arabidopsis RING E3 ligase exhibiting dual targeting of its splice isoforms, is involved in ethylene-mediated regulation of apical hook curvature. Mol Plant **5:** 1295–1309

Chau V, Tobias JW, Bachmair A, Marriott D, Ecker DJ, Gonda DK, Varshavsky A (1989) A multiubiquitin chain is confined to specific lysine in a targeted short-lived protein. Science **243:** 1576–1583

Cheng PL, Lu H, Shelly M, Gao H, Poo MM (2011) Phosphorylation of E3 ligase Smurf1 switches its substrate preference in support of axon development. Neuron **69:** 231–243

Ching SL, Gidda SK, Rochon A, van Cauwenberghe OR, Shelp BJ, Mullen RT (2012) Glyoxylate reductase isoform 1 is localized in the cytosol and not peroxisomes in plant cells. J Integr Plant Biol **54:** 152–168

Chomczynski P, Sacchi N (1987) Single-step method of RNA isolation by acid guanidinium thiocyanate-phenol-chloroform extraction. Anal Biochem **162:** 156–159

Clough SJ, Bent AF (1998) Floral dip: a simplified method for Agrobacterium-mediated transformation of Arabidopsis thaliana. Plant J **16:** 735–743

de Bie P, Ciechanover A (2011) Ubiquitination of E3 ligases: self-regulation of the ubiquitin system via proteolytic and non-proteolytic mechanisms. Cell Death Differ **18:** 1393–1402

Deng L, Wang C, Spencer E, Yang L, Braun A, You J, Slaughter C, Pickart C, Chen ZJ (2000) Activation of the IkappaB kinase complex by TRAF6 requires a dimeric ubiquitin-conjugating enzyme complex and a unique polyubiquitin chain. Cell **103:** 351–361

Deshaies RJ, Joazeiro CA (2009) RING domain E3 ubiquitin ligases. Annu Rev Biochem **78:** 399–434

Dou H, Buetow L, Hock A, Sibbet GJ, Vousden KH, Huang DT (2012) Structural basis for autoinhibition and phosphorylation-dependent activation of c-Cbl. Nat Struct Mol Biol **19:** 184–192

Durek P, Schmidt R, Heazlewood JL, Jones A, MacLean D, Nagel A, Kersten B, Schulze WX (2010) PhosPhAt: the Arabidopsis thaliana phosphorylation site database. An update. Nucleic Acids Res **38:** D828–D834

Earley KW, Haag JR, Pontes O, Opper K, Juehne T, Song K, Pikaard CS (2006) Gateway-compatible vectors for plant functional genomics and proteomics. Plant J **45:** 616–629

Engelsberger WR, Schulze WX (2012) Nitrate and ammonium lead to distinct global dynamic phosphorylation patterns when resupplied to nitrogen-starved Arabidopsis seedlings. Plant J **69:** 978–995

Frei dit Frey N, Robatzek S (2009) Trafficking vesicles: pro or contra pathogens? Curr Opin Plant Biol **12:** 437–443

Geng J, Shin ME, Gilbert PM, Collins RN, Burd CG (2005) Saccharomyces cerevisiae Rab-GDI displacement factor ortholog Yip3p forms distinct complexes with the Ypt1 Rab GTPase and the reticulon Rtn1p. Eukaryot Cell **4:** 1166–1174

Genschik P, Criqui MC, Parmentier Y, Derevier A, Fleck J (1998) Cell cycle-dependent proteolysis in plants: identification of the destruction box pathway and metaphase arrest produced by the proteasome inhibitor mg132. Plant Cell **10:** 2063–2076

Heo JB, Bang WY, Kim SW, Hwang SM, Son YS, Im CH, Acharya BR, Kim CW, Kim SW, Lee BH, et al (2010) OsPRA1 plays a significant role in targeting of OsRab7 into the tonoplast via the prevacuolar compartment during vacuolar trafficking in plant cells. Planta **232:** 861–871

Huang X, Liu X, Chen X, Snyder A, Song WY (2013) Members of the XB3 family from diverse plant species induce programmed cell death in *Nicotiana benthamiana*. PLoS ONE **8:** e63868

Hunter T (2007) The age of crosstalk: phosphorylation, ubiquitination, and beyond. Mol Cell **28:** 730–738

Huysmans M, Lema A S, Coll NS, Nowack MK (2017) Dying two deaths: programmed cell death regulation in development and disease. Curr Opin Plant Biol **35:** 37–44

Ishiga Y, Ishiga T, Uppalapati SR, Mysore KS (2011) Arabidopsis seedling flood-inoculation technique: a rapid and reliable assay for studying plant-bacterial interactions. Plant Methods **7:** 32

Kamei CLA, Boruc J, Vandepoele K, Van den Daele H, Maes S, Russinova E, Inzé D, De Veylder L (2008) The PRA1 gene family in Arabidopsis. Plant Physiol **147:** 1735–1749

Komander D, Rape M (2012) The ubiquitin code. Annu Rev Biochem **81:** 203–229

Kraft E, Stone SL, Ma L, Su N, Gao Y, Lau OS, Deng XW, Callis J (2005) Genome analysis and functional characterization of the E2 and RING-type E3 ligase ubiquitination enzymes of Arabidopsis. Plant Physiol **139:** 1597–1611

Lee MH, Jung C, Lee J, Kim SY, Lee Y, Hwang I (2011) An Arabidopsis prenylated Rab acceptor 1 isoform, AtPRA1.B6, displays differential inhibitory effects on anterograde trafficking of proteins at the endoplasmic reticulum. Plant Physiol **157:** 645–658

Lingard MJ, Gidda SK, Bingham S, Rothstein SJ, Mullen RT, Trelease RN (2008) *Arabidopsis* PEROXIN11c-e, FISSION1b, and DYNAMIN-RELATED PROTEIN3A cooperate in cell cycle-associated replication of peroxisomes. Plant Cell **20:** 1567–1585

Liu H, Stone SL (2010) Abscisic acid increases *Arabidopsis* ABI5 transcription factor levels by promoting KEG E3 ligase self-ubiquitination and proteasomal degradation. Plant Cell **22:** 2630–2641

Liu H, Stone SL (2013) Cytoplasmic degradation of the Arabidopsis transcription factor abscisic acid insensitive 5 is mediated by the RING-type E3 ligase KEEP ON GOING. J Biol Chem **288:** 20267–20279

Liu H, Wang Y, Xu J, Su T, Liu G, Ren D (2008) Ethylene signaling is required for the acceleration of cell death induced by the activation of AtMEK5 in Arabidopsis. Cell Res **18:** 422–432

Lu D, Lin W, Gao X, Wu S, Cheng C, Avila J, Heese A, Devarenne TP, He P, Shan L (2011) Direct ubiquitination of pattern recognition receptor FLS2 attenuates plant innate immunity. Science **332:** 1439–1442

Lu Q, Tang X, Tian G, Wang F, Liu K, Nguyen V, Kohalmi SE, Keller WA, Tsang EW, Harada JJ, et al (2010) Arabidopsis homolog of the yeast TREX-2 mRNA export complex: components and anchoring nucleoporin. Plant J **61:** 259–270

Lyzenga WJ, Booth JK, Stone SL (2012) The Arabidopsis RING-type E3 ligase XBAT32 mediates the proteasomal degradation of the ethylene biosynthetic enzyme, 1-aminocyclopropane-1-carboxylate synthase 7. Plant J **71:** 23–34

Munch D, Teh OK, Malinovsky FG, Liu Q, Vetukuri RR, El Kasmi F, Brodersen P, Hara-Nishimura I, Dangl JL, Petersen M, Mundy J, Hofius D (2015) Retromer contributes to immunity-associated cell death in Arabidopsis. Plant Cell **27:** 463–479

Nelson BK, Cai X, Nebenführ A (2007) A multicolored set of in vivo organelle markers for co-localization studies in Arabidopsis and other plants. Plant J **51:** 1126–1136

Nodzon LA, Xu WH, Wang Y, Pi LY, Chakrabarty PK, Song WY (2004) The ubiquitin ligase XBAT32 regulates lateral root development in Arabidopsis. Plant J **40:** 996–1006

Nomura K, Mecey C, Lee YN, Imboden LA, Chang JH, He SY (2011) Effector-triggered immunity blocks pathogen degradation of an immunity-associated vesicle traffic regulator in Arabidopsis. Proc Natl Acad Sci USA **108:** 10774–10779

Pecenková T, Hála M, Kulich I, Kocourková D, Drdová E, Fendrych M, Toupalová H, Zársky V (2011) The role for the exocyst complex subunits Exo70B2 and Exo70H1 in the plant-pathogen interaction. J Exp Bot **62:** 2107–2116

Peng J, Schwartz D, Elias JE, Thoreen CC, Cheng D, Marsischky G, Roelofs J, Finley D, Gygi SP (2003) A proteomics approach to understanding protein ubiquitination. Nat Biotechnol **21:** 921–926

Petersen NH, Joensen J, McKinney LV, Brodersen P, Petersen M, Hofius D, Mundy J (2009) Identification of proteins interacting with Arabidopsis ACD11. J Plant Physiol **166:** 661–666

Prasad ME, Schofield A, Lyzenga W, Liu H, Stone SL (2010) Arabidopsis RING E3 ligase XBAT32 regulates lateral root production through its role in ethylene biosynthesis. Plant Physiol **153:** 1587–1596

Prasad ME, Stone SL (2010) Further analysis of XBAT32, an Arabidopsis RING E3 ligase, involved in ethylene biosynthesis. Plant Signal Behav **5:** 1425–1429

Rock KL, Gramm C, Rothstein L, Clark K, Stein R, Dick L, Hwang D, Goldberg AL (1994) Inhibitors of the proteasome block the degradation of most cell proteins and the generation of peptides presented on MHC class I molecules. Cell **78:** 761–771

Ronald PC, Albano B, Tabien R, Abenes L, Wu KS, McCouch S, Tanksley SD (1992) Genetic and physical analysis of the rice bacterial blight disease resistance locus, Xa21. Mol Gen Genet **236:** 113–120

Sadanandom A, Bailey M, Ewan R, Lee J, Nelis S (2012) The ubiquitin-proteasome system: central modifier of plant signalling. New Phytol **196:** 13–28

Smalle J, Vierstra RD (2004) The ubiquitin 26S proteasome proteolytic pathway. Annu Rev Plant Biol **55:** 555–590

Song WY, Wang GL, Chen LL, Kim HS, Pi LY, Holsten T, Gardner J, Wang B, Zhai WX, Zhu LH, et al (1995) A receptor kinase-like protein encoded by the rice disease resistance gene, Xa21. Science **270:** 1804–1806

Sparkes IA, Runions J, Kearns A, Hawes C (2006) Rapid, transient expression of fluorescent fusion proteins in tobacco plants and generation of stably transformed plants. Nat Protoc **1:** 2019–2025

Stegmann M, Anderson RG, Ichimura K, Pecenkova T, Reuter P, Žársky V, McDowell JM, Shirasu K, Trujillo M (2012) The ubiquitin ligase PUB22 targets a subunit of the exocyst complex required for PAMP-triggered responses in *Arabidopsis*. Plant Cell **24:** 4703–4716

Stone SL (2014) The role of ubiquitin and the 26S proteasome in plant abiotic stress signaling. Front Plant Sci **5:** 135

Stone SL, Hauksdóttir H, Troy A, Herschleb J, Kraft E, Callis J (2005) Functional analysis of the RING-type ubiquitin ligase family of Arabidopsis. Plant Physiol **137:** 13–30

Stone SL, Williams LA, Farmer LM, Vierstra RD, Callis J (2006) KEEP ON GOING, a RING E3 ligase essential for *Arabidopsis* growth and development, is involved in abscisic acid signaling. Plant Cell **18:** 3415–3428

Swaney DL, Beltrao P, Starita L, Guo A, Rush J, Fields S, Krogan NJ, Villén J (2013) Global analysis of phosphorylation and ubiquitylation cross-talk in protein degradation. Nat Methods **10:** 676–682

Thacker JS, Yeung DH, Staines WR, Mielke JG (2016) Total protein or high-abundance protein: Which offers the best loading control for Western blotting? Anal Biochem **496:** 76–78

Thrower JS, Hoffman L, Rechsteiner M, Pickart CM (2000) Recognition of the polyubiquitin proteolytic signal. EMBO J **19:** 94–102

Vierstra RD (2009) The ubiquitin-26S proteasome system at the nexus of plant biology. Nat Rev Mol Cell Biol **10:** 385–397

Wang F, Zhu D, Huang X, Li S, Gong Y, Yao Q, Fu X, Fan LM, Deng XW (2009) Biochemical insights on degradation of *Arabidopsis* DELLA proteins gained from a cell-free assay system. Plant Cell **21:** 2378–2390

Wang YS, Pi LY, Chen X, Chakrabarty PK, Jiang J, De Leon AL, Liu GZ, Li L, Benny U, Oard J, et al (2006) Rice XA21 binding protein 3 is a ubiquitin ligase required for full Xa21-mediated disease resistance. Plant Cell **18:** 3635–3646

Xu P, Duong DM, Seyfried NT, Cheng D, Xie Y, Robert J, Rush J, Hochstrasser M, Finley D, Peng J (2009) Quantitative proteomics reveals the function of unconventional ubiquitin chains in proteasomal degradation. Cell **137:** 133–145

Yang C, Zhou W, Jeon MS, Demydenko D, Harada Y, Zhou H, Liu YC (2006) Negative regulation of the E3 ubiquitin ligase itch via Fyn-mediated tyrosine phosphorylation. Mol Cell **21:** 135–141

Yuan X, Zhang S, Liu S, Yu M, Su H, Shu H, Li X (2013) Global analysis of ankyrin repeat domain C3HC4-type RING finger gene family in plants. PLoS ONE **8:** e58003

Zipfel C, Robatzek S, Navarro L, Oakeley EJ, Jones JD, Felix G, Boller T (2004) Bacterial disease resistance in Arabidopsis through flagellin perception. Nature **428:** 764–767